RESEARCH ARTICLE | MARCH 06 2024

A one-way coupling approach for simulating in-nozzle flow and spray characteristics of a pressure-swirl atomizer

Zongyu Yue (岳宗宇) ; Heng Liu (刘恒) ; Chuang Gao (高闯); Song Cheng (成松) ; Hu Wang (王泮) ; Zunqing Zheng (郑尊清) ; Mingfa Yao (尧命发)

Physics of Fluids 36, 033314 (2024)
https://doi.org/10.1063/5.0194007

Physics of Fluids ARTICLE pubs.aip.org/aip/pof

A one-way coupling approach for simulating in-nozzle flow and spray characteristics of a pressure-swirl atomizer

Cite as: Phys. Fluids **36**, 033314 (2024); doi: 10.1063/5.0194007
Submitted: 25 December 2023 · Accepted: 4 February 2024 ·
Published Online: 6 March 2024

Zongyu Yue (岳宗宇),[1] Heng Liu (刘恒),[1,a)] Chuang Gao (高闯),[2,b)] Song Cheng (成松),[3] Hu Wang (王浒),[1] Zunqing Zheng (郑尊清),[1] and Mingfa Yao (尧命发)[1]

AFFILIATIONS

[1]State Key Laboratory of Engines, Tianjin University, Tianjin 300072, China
[2]Shanghai Advanced Research Institute, Chinese Academy of Sciences, Shanghai 201210, China
[3]Department of Mechanical Engineering, The Hong Kong Polytechnic University, Kowloon, Hong Kong, China

[a)]**Author to whom correspondence should be addressed:** liu_heng@tju.edu.cn
[b)]**Electronic mail:** gaoc@sari.ac.cn

ABSTRACT

This article proposes a model framework coupling in-nozzle flow and external spray and presents its application to the simulation of a commercial pressure-swirl atomizer, focusing on the transient characteristics of the internal flow and subsequently the impact on the spray characteristics. High-fidelity in-nozzle simulation of the liquid–gas interactions is performed using the volume-of-fluid (VOF) method. Then, a corresponding Lagrangian simulation of sprays is performed where the parcels are injected using the information from the VOF predictions instead of phenomenological models. Both the internal flow and the spray are compared to the experimental data that are available in the literature, and satisfactory agreement is obtained in terms of the in-nozzle velocity, film thickness, and Sauter mean diameter. The effect of the different liquid properties and geometric features on the air–core formation, and consequently, on the spray characteristics have been obtained directly through spray simulation coupled with nozzle flow. As indicated by the Eulerian simulation results, the viscosity plays a key role in the formation of the air core, as the hollow-cone shape can degenerate into a solid cylindrical liquid jet under high viscosity conditions. Additionally, significantly distinct spray characteristics in terms of droplet velocity, mean diameter, and penetration were predicted depending on the formation of air core. Even if there is no stable air core in the nozzle, the spray is still discharged in a swirling motion. As opposed to the converging angle and orifice length, the nozzle diameter has a direct correlation with the formation of air core and spray atomization. This study implies that the in-nozzle flow field, which is usually ignored in fuel spray simulation, has a substantial impact on the spray characteristics and should be taken into account for design optimization by applying the developed one-way coupling approach.

I. INTRODUCTION

Pressure-swirl (PS) atomizers are widely used in gas turbine engines,[1] internal combustion engines,[2] spray cooling,[3] and other industrial applications[4,5] due to the simple structure and excellent atomization performance. The basic structure of PS atomizer usually consists of several tangential ports, a swirl chamber, a convergent section, and an exit orifice. Typically, the liquid enters the swirl chamber via tangential ports where it gains high swirl velocity. The swirling liquid is accelerated while flowing through the convergent section. Furthermore, the air core can be formed under specific conditions, and then the liquid sheet goes through primary breakup and secondary breakup to form disintegrated liquid droplets. Despite the simple geometry, the in-nozzle flow is complex and impacted by a number of factors such as liquid properties, nozzle structures, flow field and pressure distribution especially at nozzle exit, which are essential in determining the spray atomization process.

Numerous studies have shown that the nozzle geometry directly affects the in-nozzle flow and subsequently the spray characteristics. Experiments such as that conducted by Halder *et al.*[6] on 21 transparent PS atomizers have shown that the Reynolds number and the nozzle geometry can affect the shape and the size of a fully developed air core. Cui *et al.*[7] conducted a study examining the impact of geometric deviations in orifices. The in-nozzle flow was visualized and examined how it impacts the spray characteristics, showing that the smaller cylindrical

nozzle has inhibitive effect on air–core development. Wei and Yong[8] analyzed the impact of geometrical variations on Sauter mean diameter (SMD) among 18 PS atomizers, showing that the SMD increases with the increase in tangential port area. It was also found that the smaller the spray cone angle and the thicker the film at the injector exit, the larger the SMD.

Computational fluid dynamics (CFD) plays a vital role in revealing the complex phenomena at in- and near-nozzle dense regions of atomizers, especially for realistic small-scale nozzles that are challenging for optical diagnostics. Volume of fluid (VOF) methods can be employed to simulate two-phase flow and sprays which solve the transport function of void fraction and construct the interface between liquid and gas using either piecewise linear interface construction (PLIC)[9] or high resolution interface capturing (HRIC) scheme.[10] Liu *et al.*[11] employed a VOF method to predict the perforation disintegration process and atomization characteristics of the swirl liquid sheet. However, these approaches usually need micro-level refined mesh resolution to capture the air–core interface and resolve the disintegrated liquid droplets, which are prohibitively expensive in computational resources for simulation of full-scale spray and combustion problems. To address these challenges, the discrete droplet method (DDM) has been developed and used for decades[12,13] to model the process of liquid spray atomization. In this approach, liquids are grouped and represented by Lagrangian parcels. The primary breakup of the intact liquid core and the secondary breakup of the drops can be modeled by methods such as Kelvin–Helmholtz (KH), Rayleigh–Taylor (RT), Taylor analogy breakup (TAB), and so on. Sim *et al.*[14] applied the Lagrangian discrete parcel model to simulate outwardly opening injectors and performed detailed analysis on the aerodynamic breakup process of a hollow-cone spray. However, the initialization of the injected parcels is usually based on semi-empirical models or experimental measurement data and neglects the impacts of in-nozzle flows, which considerably reduces the predictability of the model.

It is generally understood that the Eulerian–Eulerian approach can provide detailed information of the two-phase flow yet it is more expensive than Eulerian–Lagrangian approach. Therefore, coupling these two approaches for spray simulation is promising because it could take advantage of both. One type of approaches coupling Eulerian and Lagrangian framework is Eulerian–Lagrangian spray atomization (ELSA). In this approach fully Eulerian (mixture multiphase) is applied in the near-nozzle regions while farther downstream the framework switches to Eulerian–Lagrangian. Different models based on Eulerian framework for atomization have been studied, e.g., the Σ–Y model proposed by Vallet *et al.*[15] can be applied to simulate near-nozzle dense regions. Later on, Demoulin *et al.*[16] coupled the Σ–Y model with a Lagrangian description of the spray, wherein the primary breakup is achieved. The transition from the Eulerian solution to Lagrangian simulation downstream is performed based on the interface surface density. Hoyas *et al.*[17] employed ELSA model to simulate the whole spray evolution and accurately captured many of the most important characteristics of the spray, such as penetration and the axial velocity. This coupling approach simulates both continuous phase and discrete phase fluids simultaneously, hence can be referred to as an online coupling approach. This approach can extend the physical length scales while maintaining accuracy during the whole spray simulation. However, the step for time-marching for the online coupling approach is still limited by the Eulerian simulation (10^{-9} to 10^{-8} s), while typical full-scale spray and combustion simulation with the Lagrangian approach usually use large time step (10^{-7} to 10^{-6} s). Thus, it remains challenging for the online coupling approach to extend into efficient simulations of realistic spray combustion problems.

On the other hand, an off-line one-way coupling approach was developed[18] by employing the in-nozzle simulation result as an input for the following Lagrangian spray simulation, and it produced better predictions for the near-nozzle dense mixture distributions.[19,20] Most of studies within this topic concentrated on the sprays from the engine combustion network (ECN). Wang *et al.*[21] conducted the diesel spray simulations coupled with cavitating flow, showing that compared to the conventional rate-of-injection (ROI) simulation, the spray structure of coupling simulation appeared asymmetric characteristic with much larger spray cone angle and shorter spray penetration. Al-lehaibi *et al.*[22] investigated the spray and combustion characteristics of the Spray A, C, and D injections using the one-way coupling approach in commercial software CONVERGE.[18] The simulation results agree well with the experimental data in terms of the projected density, mass flow rates, spray penetrations, mixture distributions, and ignition delays. Nocivelli *et al.*[23] simulated the ECN Spray G using a homogeneous relaxation model (HRM) to predict the in-nozzle flow, which was then used to initialize Lagrangian spray simulation. The results show that one-way coupling model can capture the correct spray spatial and temporal evolution of the liquid jets at fully open needle conditions but lack accuracy in the injector opening and closing transients.

The application of one-way coupling approach to the simulation of PS atomizers is so far still rare to see. In fact, the commercial implementation such as the one in software CONVERGE is only suitable for solid cone sprays and cannot be directly applied to hollow cone sprays generated from PS atomizer. Ju *et al.*[24] attempted to model a PS atomizer with the one-way coupling approach. In their work, a mixture model is used and an effective liquid film is defined, but the results show that the spray cone angles are underestimated. Therefore, the one-way coupling approach still requires further development to be applied to PS atomizer sprays with hollow cone structure.

In this study, a high-fidelity simulation of the liquid–gas interactions within the PS atomizers is performed using the volume-of-fluid (VOF) method coupled with the Geo-reconstruct method. Then, a novel Euler–Lagrangian one-way coupling method was developed for PS atomizers, wherein the injected parcels are initialized using the data from high-fidelity nozzle flow simulation instead of phenomenological models. Both the internal flow and the spray characteristics are compared with the experimental data available in the literature, and satisfactory agreements are obtained since the one-way coupling approach has the advantage over traditional Lagrangian model for prediction of spray distribution at the nozzle exit. Furthermore, the effects of multiple parameters on the air–core formation and subsequently on the spray characteristics have been obtained directly through spray simulation coupled with nozzle flow.

II. NUMERICAL METHODS

A. In-nozzle flow field model

The VOF method[25] is applied to solve the gas–liquid two-phase flow within the PS atomizer and the near-nozzle dense spray. In this method, both fluids are assumed to be incompressible and resolved on a computational mesh. The velocity difference across the interphase

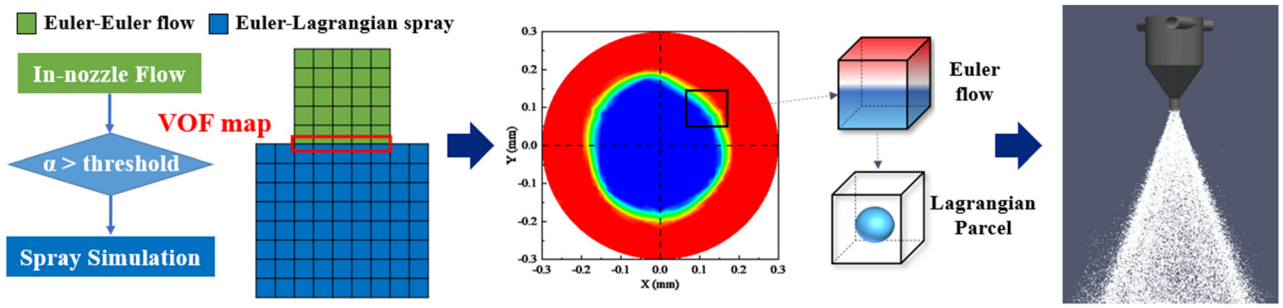

FIG. 1. Schematic of the one-way coupling model.

inside a single computational cell is neglected. The government equation reads as follows:

$$\rho\left(\frac{\partial \mathbf{u}}{\partial t}+\mathbf{u}\cdot\nabla\mathbf{u}\right)=-\nabla p+\nabla\cdot\left(\mu\nabla\mathbf{u}+\mu(\nabla\mathbf{u})^{T}\right)+\sigma\kappa\delta_{S}\mathbf{n}, \quad (1)$$

where μ is the velocity field, ρ is the density, p is the pressure, μ is the viscosity, σ is the surface tension, κ is the local interface curvature, δ_S is a Dirac distribution concentrated at interface **S**, and **n** is a unit vector normal to the interface. The surface tension term is modeled with the continuum surface force model. In a cell where both phases exist, the following equation holds:

$$\rho=\rho_{l}\alpha+\rho_{g}(1-\alpha), \quad (2)$$

$$\mu=\mu_{l}\alpha+\mu_{g}(1-\alpha). \quad (3)$$

The subscripts g and l indicate gas phase and liquid phase, respectively; α is the void fraction in a cell. In the VOF method, the transport equation for α is solved for the two-phase immiscible incompressible flows

$$\frac{\partial\alpha}{\partial t}+\boldsymbol{u}\cdot\nabla\alpha=0. \quad (4)$$

In addition, the piecewise-linear interface calculation (PLIC) scheme is applied to capture the sharp interface between air–liquid interactions. A Pressure-Implicit with Splitting of Operators (PISO)-based scheme is used for solving the pressure–velocity coupling. A laminar flow regime is assumed since the swirl dominant flow itself tends to luminaries the flow, as indicated by Chinn *et al.*[26] The second-order upwind scheme is used to discretize the convective terms, and the first-order temporal discretization with Courant number of 0.15 is used to ensure stability.

B. One-way coupling model

The main idea of the one-way coupling method is to compute the internal flow using the VOF method, and the data of flow conditions of both phases near the nozzle orifice are recorded at a user-defined time frequency. After the VOF simulation is finished, a corresponding EL simulation of sprays in a large domain is performed, and the parcels are injected using the information from the VOF simulation. In the EL framework, the liquid film of the spray is described through a series of blobs (also called ligaments), while droplets are subsequently detached downstream. The approach is already known for engineering and widely used in literatures.[27–30] The EL simulation is performed using CONVERGE 3.0 leveraging its advanced meshing ability for complex geometry.

The schematic of the one-way coupling model is shown in Fig. 1. First, the cell information on the cross section near the nozzle exit, including the nozzle diameter, the mass flow rate of each phase across the interface, the cell centroid coordinates, the cell velocity in x, y, and z directions, the volume fraction of the liquid phase of the cell, the derived contraction coefficient *Ca* and other variables are recorded at a fixed time step.

The transition of continuous liquid into discrete parcels employs the approach introduced in CONVERGE manual[18] as follows.

(1) At a given step, if the cells with a liquid volume fraction greater than the user-defined threshold, at least one particle will be ejected at the corresponding position. Otherwise, the cells with a liquid volume fraction smaller or equal to the threshold will not inject any parcels due to the very small amount of liquid fuel.
(2) Traverse the liquid volume fractions of all grids in the map, and sum the liquid volume fraction which greater than the threshold.
(3) Divide the time-integrated total liquid mass across the region interface by the sum of the acceptable liquid volume fraction determined in step 2. The result is the mass per unit volume fraction and guarantees that cells with larger liquid volume fraction do inject more mass.
(4) Multiply the mass per unit volume fraction by the liquid volume fraction of each cell, and the result is the mass that needs to be injected into each cell.
(5) The injected parcel position will be perturbed using random numbers and limited inside a box with length, width, and height of *dx*, *dy*, and *dz*, i.e., inside the VOF grid.

For the hollow cone spray, the derived contraction coefficient *Ca* is calculated through Eq. (5) to ensure that the initial parcel diameter is equal to the liquid film thickness at the nozzle exit. R and r are the radius of orifice and air core, respectively. d_o and D are the diameter of parcels and orifice, respectively. The cross-sectional area of the air–core is assumed to be circular, allowing for the determination of r through the accumulation of the cell areas where the liquid volume fraction remains below a specified threshold

$$Ca=\frac{1}{4}\left(\frac{R-r}{R}\right)^{2}, \quad (5)$$

$$d_{o}=\sqrt{Ca}\cdot D. \quad (6)$$

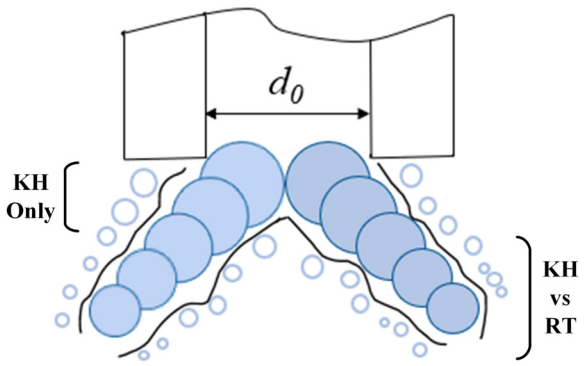

FIG. 2. Schematic of the modified KH–RT spray breakup model.

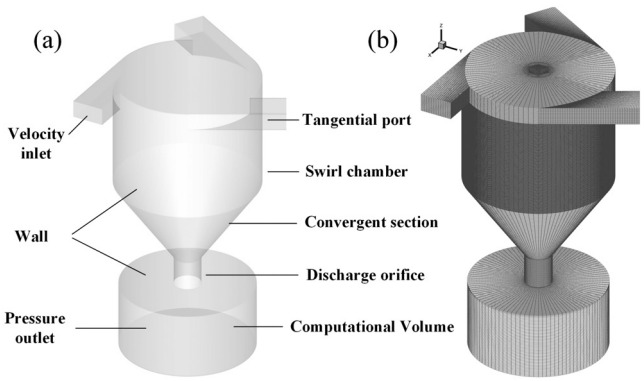

FIG. 3. The computational domain scheme of pressure swirl atomizer (a) geometry scheme and (b) mesh scheme.

According to Gao *et al.*,[31] for the hollow cone spray, the Kelvin–Helmholtz Rayleigh–Taylor (KH–RT) model[32] performs better at above-atmospheric pressure conditions, while the linear instability analysis and Taylor analogy theory (LISA-TAB) model gives relatively better predictions for the atmospheric pressure condition. In this study, the KH–RT model (shown in Fig. 2) is adopted for the primary and secondary breakup considering the potential application of the developed model for realistic combustion problem. Once blobs are started, the aerodynamic instabilities (i.e., KH waves) are responsible for the primary breakup of the injected parent liquid blobs. Child drops are created during this process with the radius of new droplets $r_c = B_0\Lambda_{KH}$ and the breakup time $\tau_{KH} = 3.788B_1D/\Omega_{KH}\Lambda_{KH}$, where τ_{KH} and Λ_{KH} are included in the following equations:

$$\Omega_{KH} = \frac{0.34 + 0.38We^{1.5}}{(1+Oh)(1+T^{0.6})}\sqrt{\frac{\sigma}{\rho_d r^3}}, \tag{7}$$

$$\Lambda_{KH} = 9.02r\frac{\left(1+0.45\sqrt{Oh}\right)(1+0.4T^{0.7})}{(1+0.865We^{1.67})^{0.6}}, \tag{8}$$

where $Oh = \sqrt{We_l/Re_l}$ is the Ohnesorge number and $T = Oh\sqrt{We_g}$ is the Taylor number. The secondary breakup of these drops is modeled by comparing the competing effects of the KH and RT mechanisms. In addition to the models mentioned above, the Lagrangian spray simulation also features the Frossling evaporation model[33] and the no-time counter (NTC) particle collision model[34] that have previously been successfully applied in combustion engine simulations.

C. Geometry and boundary conditions

The nozzle geometry and mesh scheme of the in-nozzle computational domain are shown in Fig. 3. For the whole domain, the hexahedral cells are generated, and fixed embedded are applied surrounding the central axis to increase grid resolution within the gas–liquid two-phase flow region. Both the length and diameter of the orifice are 0.6 mm. The inlet boundary is set as velocity inlet to ensure a fuel mass flow rate of 18.5 kg/h, while the outlet is set as pressure outlet at 1.0 bar. No-slip conditions are applied to the walls.

To validate the numerical model, two other PS atomizer geometries are modeled and investigated numerically, which are a large-scale transparent nozzle by Maly *et al.*[35] and a real size metal nozzle by Jedelsky *et al.*[36] The two nozzles will be used to valid the in-nozzle flow and spray breakup, respectively, and note that the detailed in-nozzle experimental measurements are only available in large-scale nozzle. Figure 4 shows the computational domains of the nozzles for model validation. Both nozzles have three tangential inlet ports which are evenly distributed. The large-scale nozzle has a straightly converging section, while the real size one has a hemispherical-shaped swirl chamber. All the dimensions of the two nozzles are reported in Table I.

The operating fuels for three nozzles are p-cymene, jet A-1, and diesel, respectively, as seen in Table II. More details about the experimental setup can be referred to Refs. 35 and 36.

The computational domain of the external spray is shown in Fig. 5. The diameter of cylindrical computational domain is 80 mm, with a height of 40 mm. The in- and near-nozzle flow results serve as boundary conditions for the external spray simulation; thus, there is no need to define nozzle positions, flow coefficient, rate of injection (ROI) profile, and so on. The side and bottom of domain are set as the pressure outlet condition, while the top surface is considered fixed wall. The temperature and pressure of entire domain are 300 K and 1.0 bar, respectively, which are the same as experimental values.

III. MODEL VALIDATION

A. Test of grid independence

For grid-dependency study, one of the key parameters for nozzle flow is the number of mesh cells across the exit orifice which determine the accuracy of the air–core dimension. Ghate and Sundararajan[37] suggest a mesh with roughly 26 cells in orifice diameter d_o, while Galbiati *et al.*[38] found grid independence for a much finer mesh, approximately 40 50 cells in orifice radius r_o. In this study, predictions of volume fraction and velocity magnitude at 0.1 mm upstream of the nozzle exit using fine, medium, and coarse meshes are presented, corresponding to the black, red, and blue lines in Fig. 6. The total number of cells for the three mesh schemes is 4 695 042 cells, 2 502 366 cells, and 906 321 cells, corresponding to 27, 22, and 16 cells in r_o, respectively. It is seen that at a quasi-steady state, the trend of velocity and volume fraction is basically the same under three meshes. In the central air–core region of the nozzle, the velocity magnitude predicted by the three meshes shows negligible difference. In the gas–liquid two-phase region, the coarse mesh (represented by the black line) predicted a deviation in the volume fraction due to the presence of the large velocity gradients. In other words, the coarse mesh

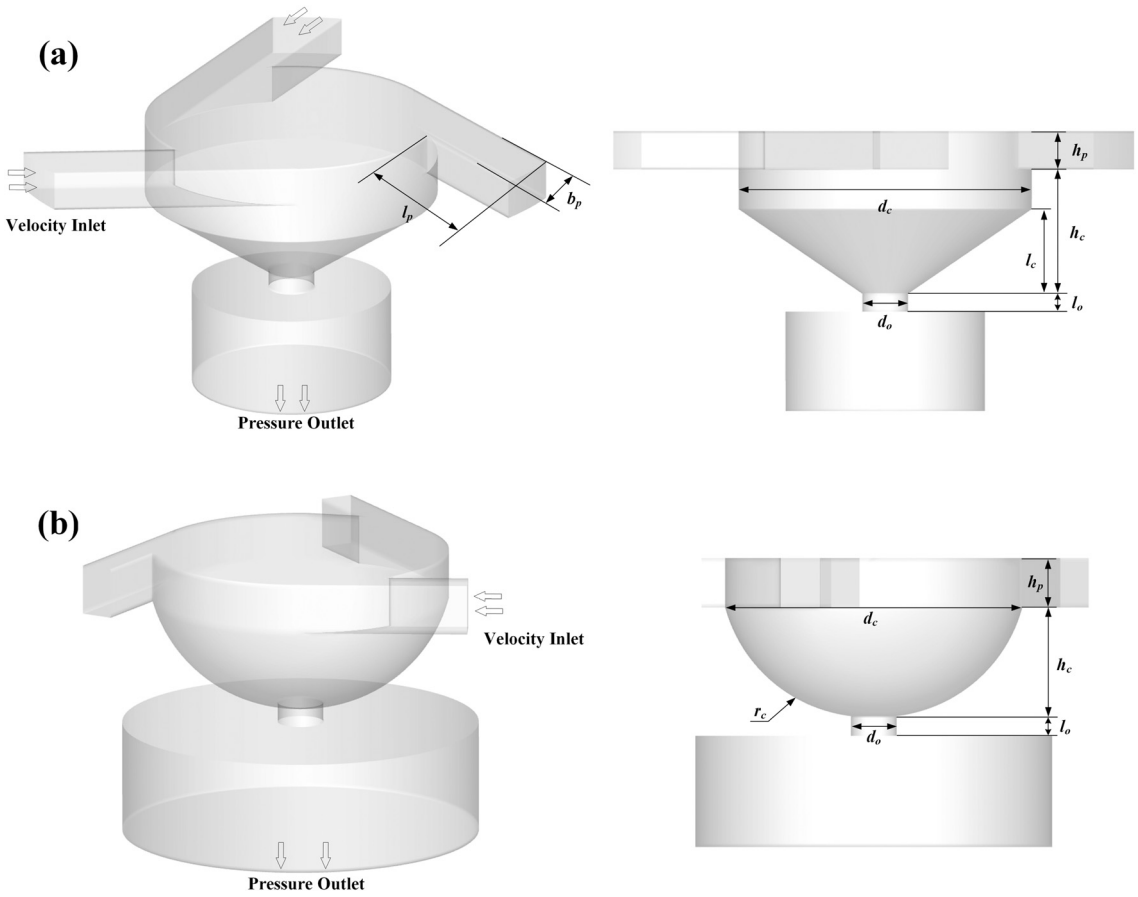

FIG. 4. Computational geometry of (a) the large-scale transparent nozzle and (b) the real size metal nozzle.

TABLE I. Geometric details of nozzles for validation.

	d_c	d_o	h_p	h_c	l_o	l_p	b_p	r_c	l_c
Milan *et al.*	29.1	4.58	3.85	12.5	1.8	15.2	6.3	…	8.5
Jedelsky *et al.*	3	0.45	0.5	1.1	0.2	0.8	0.33	1.5	…

TABLE II. Operating conditions and relevant fuel properties for testing cases.

	Large scale	Real size nozzle	This study
Fuel	P-cymene	Jet A-1	Diesel
Fuel density (kg/m^3)	848	795	848
Fuel viscosity (kg/m s)	0.000 85	0.0016	0.0027
Surface tension (kg/s^2)	0.028	0.029	0.028
Injection velocity magnitude (m/s)	0.41	5.15	7.19
Ambient pressure (bar)	1.0	1.0	1.0

underpredicts the diameter of air core due to poor resolution, while the distributions of volume fraction predicted by the medium and fine meshes are almost the same. Therefore, the medium mesh with a minimum size of grid of 13.64 μm is adopted for subsequent in-nozzle

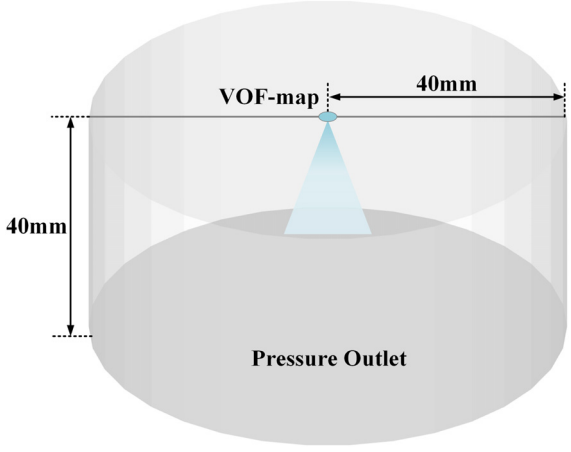

FIG. 5. The computational domain scheme of external spray.

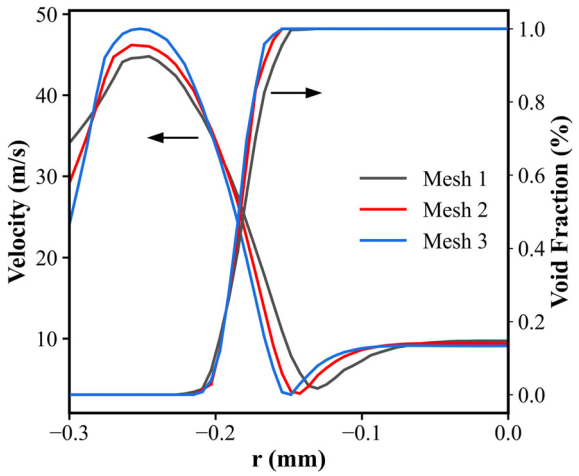

FIG. 6. The radial distribution of velocity and volume fraction with different mesh resolutions at 0.1 mm upstream of the nozzle exit.

simulation in order to achieve balance in computational cost and prediction accuracy.

Likewise, the grid dependency also plays an essential role for Eulerian–Lagrangian spray approach. The interaction of air–liquid phase cannot be accurately accounted for if using a coarse mesh, and the liquid penetration length (LPL) is typically under-predicted when there are too many injected parcels in a cell.[39] In order to determine the best mesh size for external spray simulation, a grid sensitivity test is also conducted after the in-nozzle flow simulation. Six mesh resolutions were tested using adaptive mesh refinement (AMR) which is applied to the velocity field. AMR is activated when the sub-grid velocity fluctuations rise above 0.1 m/s. Fixed grid embedding was also applied near the nozzle exit to increase grid resolution in the spray dense region. Figure 7 shows the grid dependency of the liquid penetration prediction. The predicted LPL was defined as the distance from

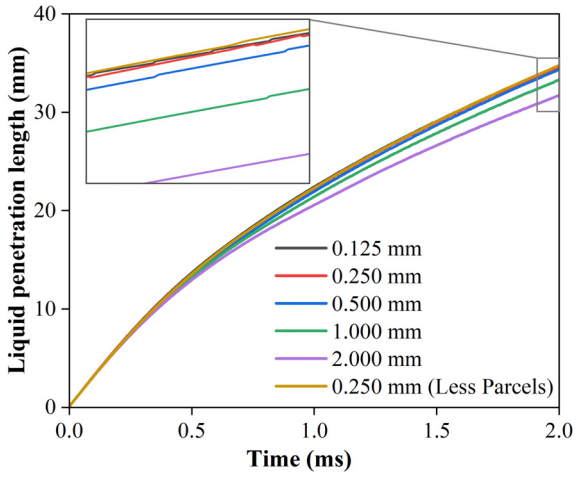

FIG. 7. Comparisons of liquid penetration length with different mesh resolutions and larger averaged mass per parcel.

the nozzle exit to the location when 95% of the total liquid mass was encompassed. With a grid size larger than 0.5 mm, the LPL is noticeably under-predicted. For cell sizes 0.25 mm and finer, the LPL prediction converges and is grid-independent. Therefore, it is concluded that an AMR mesh with a minimum cell size of 0.25 mm is sufficient to achieve grid-independence with acceptable computational cost. In addition, the sensitivity of parcel number is also tested by doubling the mass per parcel, and the results show that the parcel number effect on LPL is marginal as indicated by the comparison between the red line and the orange line in Fig. 7.

B. In-nozzle flow model validation

To verify the CFD models of in-nozzle flow, the large-scale nozzle shown in Fig. 4(a) was simulated and compared against the experimental results of Maly *et al.*[35] The radius distribution of axial and tangential velocity at axial distances of 11 and 8 mm from the atomizer cap, normalized by the mean velocity within the inlet port (v_p), is shown in Fig. 8. Red lines are the CFD results, which show excellent prediction of transient behavior, although the peak axial velocity at the bottom of swirl chamber was slightly under-predicted, as shown in Fig. 8(c). The tangential velocity increases first and decreases along the radius outward from the centerline, behaving as a Rankine vortex with a smooth transition between two flow regimes of free-vortex and solid-body rotation.[40,41]

Figure 9 shows the void fraction profile across the nozzle exit orifice and the contour of liquid volume fraction distribution. The air core is formed near the centerline of nozzle. Iso-surfaces of 0.5 void fraction are constructed to define the liquid–gas interface. Thus, the calculated diameter of air core is 0.002 69 m with a 10.03% error compared to the experimental value of 0.002 99 m. By comparing with experimental results, the accuracy of in-nozzle model is considered sufficient to capture the liquid–gas interface and is used to study the effects of operational parameters and nozzle geometry henceforth.

C. One-way coupled spray model validation

An Eulerian in-nozzle simulation of real size PS nozzle shown in Fig. 4(b) was performed first to determine the near-nozzle boundary conditions, which was then used in the validation of one-way coupled spray modeling.

Figure 10 shows the comparison of CFD predictions and experiments for spray tomography and cone angle. The predicted spray cone angle is 38.4° and exhibits a 2.78% deviation from the cone angle measured by Jedelsky *et al.*,[36] demonstrating an excellent accuracy of the developed one-way coupled spray model in predicting the macroscopic spray characteristics.

In addition to the comparison of spray cone angle, the distribution of Sauter mean diameter (SMD) along the radius at an axial location of 12.5 mm downstream of the nozzle exit is compared and shown in Fig. 11. The one-way coupled model accurately predicts the trend of SMD distribution, which initially increases and then slightly decreases along the radial direction. The value of predicted SMD matches the experiments very well especially for the spray dense region although the SMD value in the hollow region near centerline shown by experiment is not captured by the model. In addition, a numerical simulation of the external spray under the same conditions was conducted using the conventional Lagrangian model, shown as the red line in

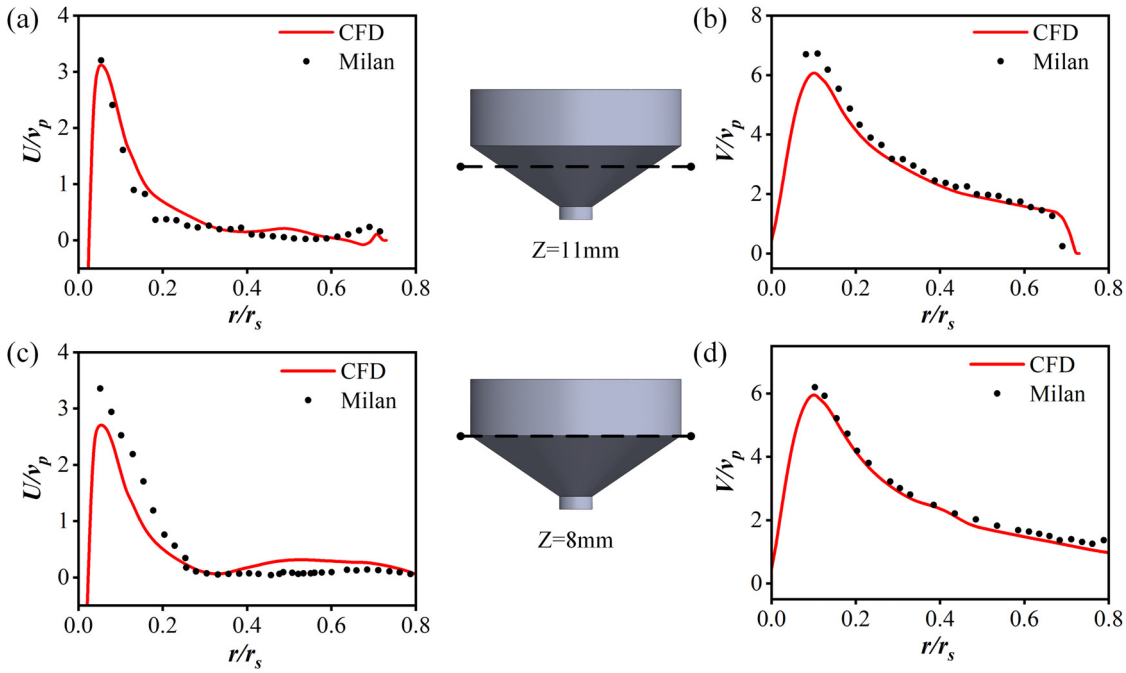

FIG. 8. Comparison of CFD predictions and experiments[35] for velocity profiles in the swirling chamber (a) and (c) axial velocity and (b) and (d) tangential velocity.

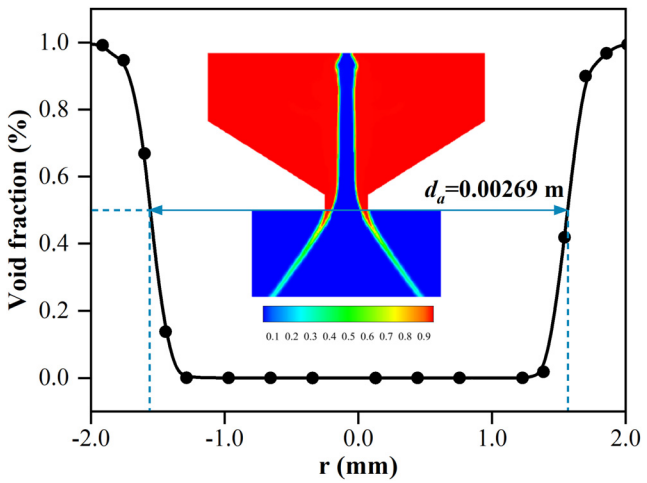

FIG. 9. The void fraction across the nozzle exit orifice.

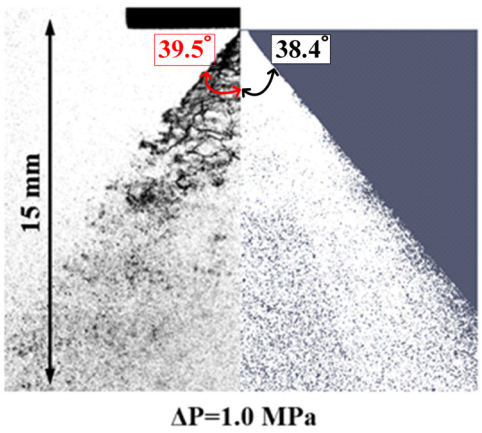

FIG. 10. Comparison of CFD predictions and experiments[36] for spray tomography and cone angle (left) experiment (right) simulation. The experimental images are reprinted with permission from Jedelsky *et al.*, Int. J. Heat Mass Transfer **121**, 788–804 (2018). Copyright 2018 Elsevier.

Fig. 11. Here, a Rosin–Rammler distribution with an initial SMD of 200 μm is applied for the injected parcels under constant injection rate. The half cone angle is set as 39.5° which is obtained from the experimental data. The constants within the KH–RT model remain unchanged compared to the one-way coupling model. In the conventional Lagrangian model, the predicted SMD is approximately 2.5 times the experimental values at the same radial position, and the width of spray distribution is significantly narrower than the experiment. While the results by conventional Lagrangian model can be definitely improved by model constant tuning, this comparison indicates the superior predictivity of the one-way coupled approach over the traditional one.

IV. RESULTS AND DISCUSSION

The hollow-cone spray characteristics can be impacted by a number of parameters such as injection pressure, nozzle structure, liquid properties, and operating conditions. In this section, the developed

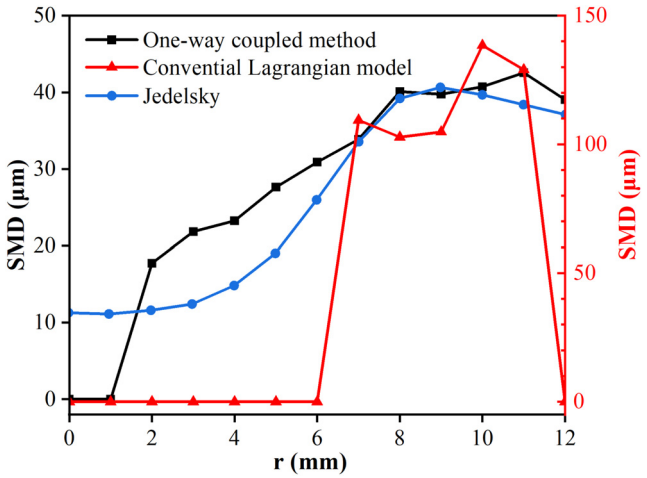

FIG. 11. Comparison of CFD predictions and experimental SMD radial distribution.

one-way coupled model is leveraged and parametric study is performed to focus on the formation of air–core inside the nozzle and, consequently, its effects on external spray characteristics. The investigated operating and geometry parameters are shown in Table III. All these cases are based on the nozzle shown in Fig. 3. For cases 7–12, the ambient pressure is set as 7.2 bar to simulate the real pressurized environment so that the results can provide valuable implications for spray process characterization and nozzle design in a real gas turbine combustor. As the orifice length decreases, the convergence angle increases accordingly from 51.4° to 59.6° keeping other geometry parameters unchanged. When the nozzle diameter changes from the baseline of 0.6 to 0.4 mm and 0.8 mm, corresponding adjustments in the swirl chamber diameter are necessary to maintain a consistent convergence angle.

A. Effects of mass flow rate

Figure 12 shows the contours of void fraction under different mass flow rate conditions (4.5, 12.3, and 18.5 kg/h). The air penetration sustains the conical shape of the liquid film as the diesel mass flow rate increases. It can be seen that the air core collapses on itself at the smallest mass flow rate, resulting in a solid cylindrical liquid jet. Due to the swirl motion, the liquid jet is not entirely straight but exhibits a distinctive crumpled shape similar to findings reported by Di Martino *et al.*[42] The disappearance of air core under diesel mass flow rate of 4.5 kg/h can be explained by the low Reynolds number at exit. Lee *et al.*[43] suggest that no air core is present inside a swirl chamber under $Re \approx 2550$ due to insufficient centrifugal forces. Here, the Reynolds number is defined as $Re = \rho v d/\mu$, where v and d are the velocity and diameter of the nozzle exit. When the diesel mass flow rate was 4.5 kg/h and the flow reached a quasi-steady state, the average velocity at the nozzle outlet cross section was 6.23 m/s, corresponding to $Re \approx 1174$, which is lower than the critical Re required for the formation of an air core.

TABLE III. Operational and geometry parameters used in the simulations.

Case	Mass flow rate (kg/h)	Viscosity (mPa s)	Orifice length (mm)	Orifice diameter (mm)
1–3	4.5, 12.3, 18.5	2.7	0.6	0.6
4–6	18.5	1.0, 2.7, 10	0.6	0.6
7–9	12.3	2.7	0.9, 0.6, 0.3	0.6
10–12	12.3	2.7	0.6	0.4, 0.6, 0.8

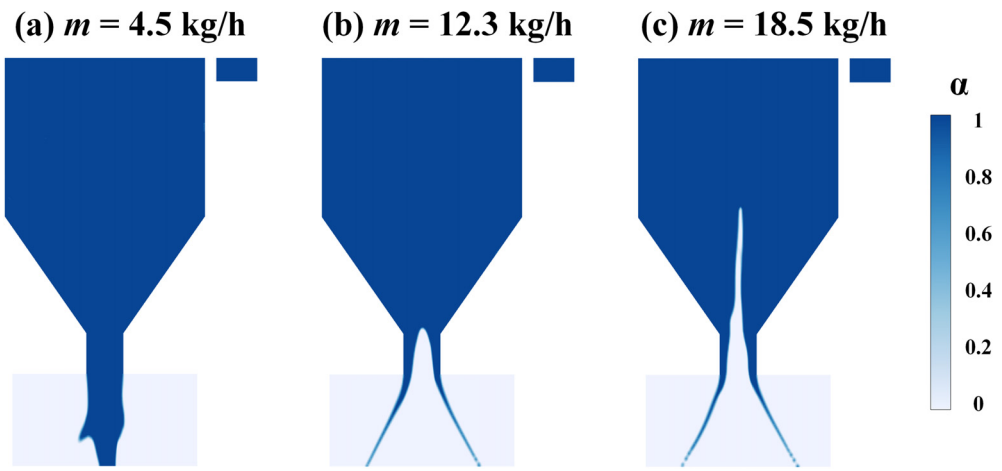

FIG. 12. Spatial distribution of void fraction under different mass flow rate.

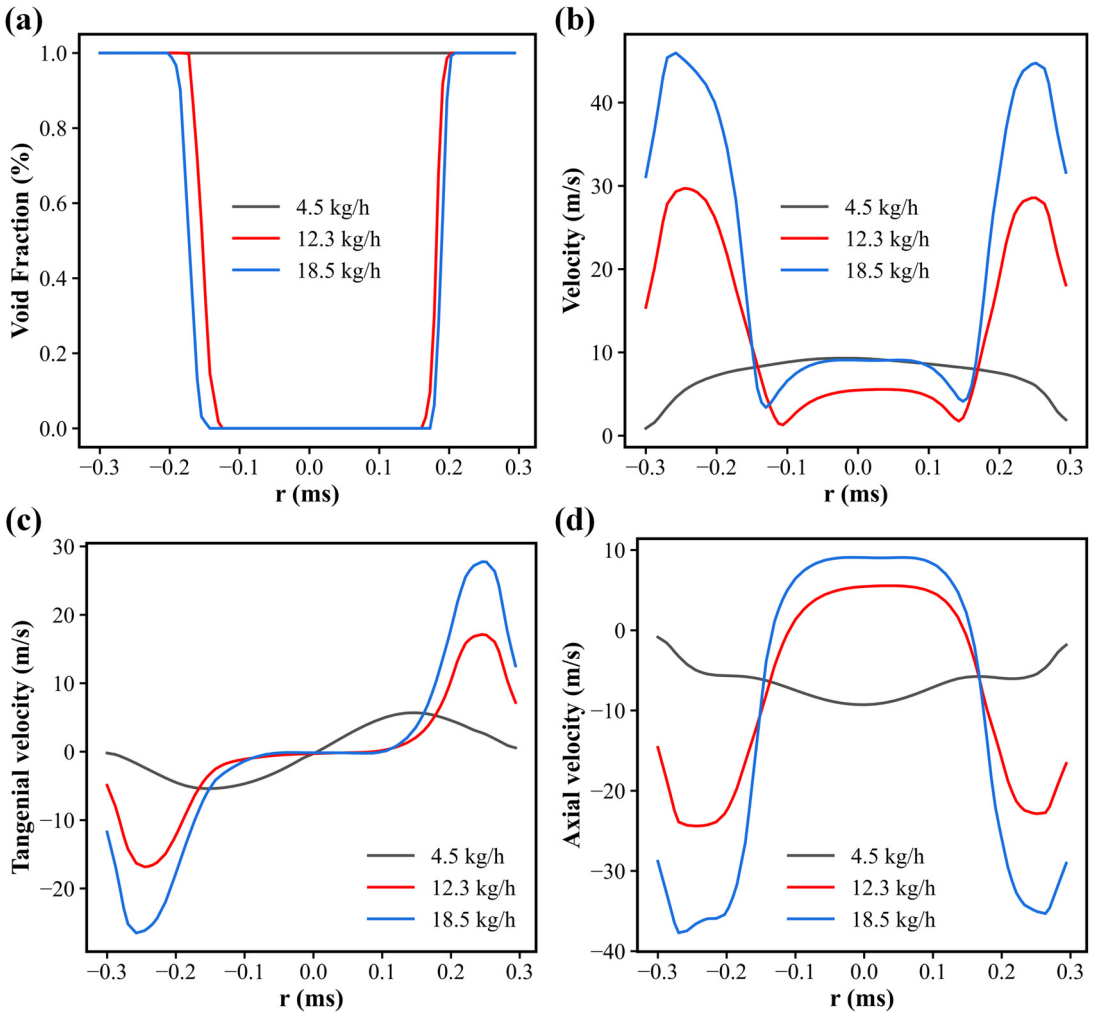

FIG. 13. The radial distribution of velocity and void fraction near the nozzle orifice under different mass flow rate (a) void fraction, (b) velocity magnitude, (c) tangential velocity, and (d) axial velocity.

Figure 13(a), the void fraction at 0.1 mm upstream of the nozzle exit, is presented under different mass flow rates. The air core exhibits an eccentric distribution possibly related to the location of inlet ports. Furthermore, the radial distributions of average velocities are shown in Fig. 13, including the absolute velocity (b), tangential velocity (c), and axial velocity (d). Near the nozzle wall, the fluid velocity is lower due to the presence of viscous layer. While in the central air core region, the gas tangential velocity is nearly zero because the air sucked into the nozzle is driven by the axial pressure difference rather than tangential force. In the case of lower diesel mass flow rate of 4.5 kg/h where no air core is established, insufficient internal gas liquid momentum exchange within the nozzle results in a velocity profile where the central region exhibits higher velocity compared to the near-wall region. The lower jet velocity is unfavorable for the breakup of external spray which will be shown later. As the diesel mass flow rate increases, the flow velocities near the nozzle exit also increase especially for liquid phase in the axial direction.

Furthermore, based on the VOF simulation data, the one-way coupling simulation for external spray is performed under different mass flow rates (4.5, 12.3, and 18.5 kg/h), and the results in clip-planes through the nozzle are shown in Fig. 14. Although a solid cylindrical liquid jet is observed under the case of 4.5 kg/h, the diesel fuel discharged from the nozzle exhibits a swirling motion and still forms a hollow cone spray as indicated by the sparse dots in the central region. At the mass flow of 18.5 kg/h, the spray retains its hollow-cone shape near the nozzle exit, but small droplets in the far field spread out by vortex induced by relative velocity difference between injected spray and quiescent air. In addition, Fig. 15 compares the predicted distributions of projected density on cross-planes near the nozzle exit and in the far field. The cross section of the hollow cone is not a regular circle. Near the nozzle exit, relatively higher density profiles are predicted near center because of the solid cylindrical liquid jet operating at 4.5 kg/h. In the far field, all cases demonstrate similar results and higher peak values are found due to the collision and coalescence of droplets.

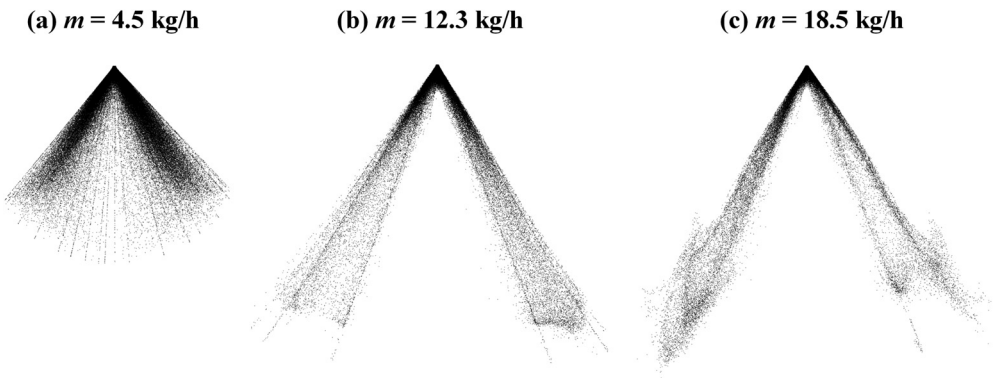

FIG. 14. Spray tomography under different mass flow rate.

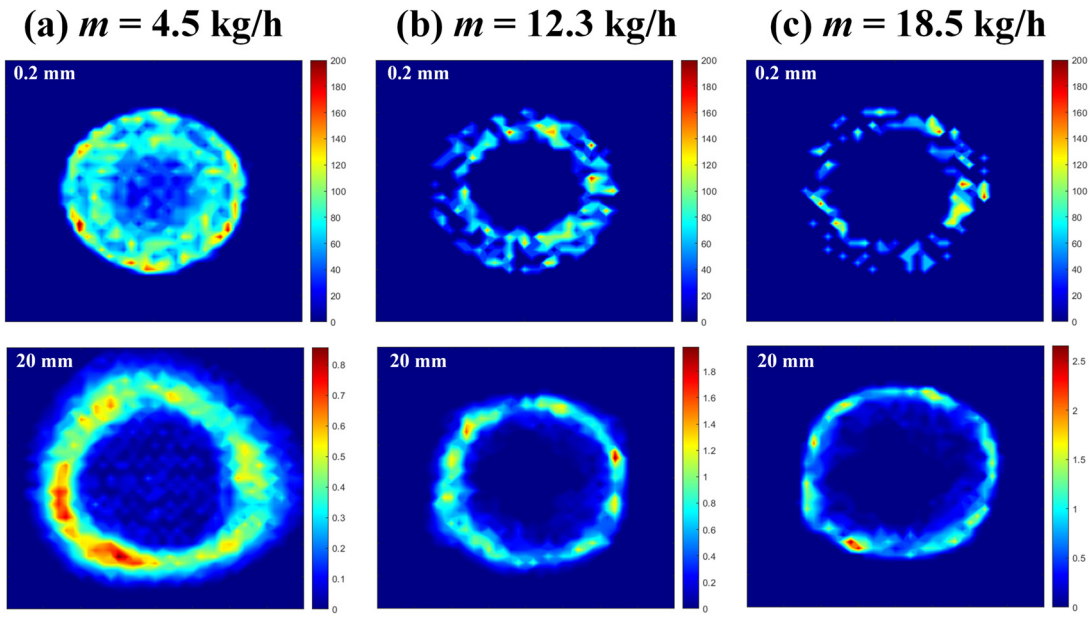

FIG. 15. Predicted distributions of projected density of external spray under different mass flow rate.

B. Effects of viscosity

In this section, an evaluation of the effects of liquid viscosity on in-nozzle flow and external spray characteristics is conducted by using one-way coupled model. Figure 16 shows the liquid spray pattern under different liquid viscosity (1.0, 2.7, and 10.0 mPa s), suggesting the significant sensitivity of air core formation on the liquid viscosity. At a liquid viscosity of 1.0 mPa s, the air core penetrates the entire nozzle and forms an umbrella-like shape at the top. As the viscosity increases, the in-nozzle air core gradually contracts and disappears. Unlike the wrinkled liquid film pattern at lower liquid viscosity, the liquid film at a liquid viscosity of 10.0 mPa s is predominantly smooth, indicating that the viscosity can suppress not only the formation of air core but also any disturbance on the liquid–gas interface.

Figure 17 compared the liquid penetration and average SMD at 15 mm downstream of the nozzle exit for different viscosity. It can be seen that the influence of liquid viscosity on the liquid penetration length is relatively minor, regardless of whether an air core forms within the nozzle. As the liquid viscosity increases, the delay for droplets to reach the sampled location remains relatively constant, while the SMD gradually increases. When the liquid viscosity increases from 2.7 to 10.0 mPa s, the SMD is increased by 170%. This is attributed to the initial diameter of parcels increases with an increased liquid film thickness near the nozzle exit due to the disappearance of the air core. In addition, the increased liquid viscosity suppresses droplet disintegration and breakup according to the KH–RT model,[32] leading to an increase in SMD.

C. Effects of nozzle geometry

Figures 18(a)–18(c) show the effects of nozzle geometry including convergence angle and orifice length (cases 7–9) on the in-nozzle flow

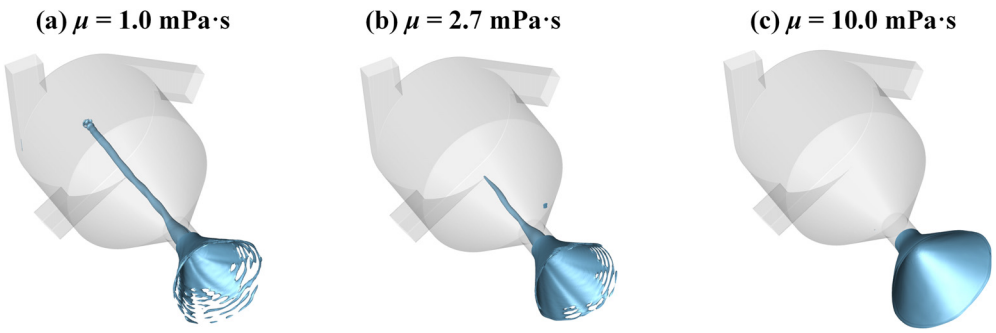

FIG. 16. Liquid spray pattern using an iso-surface of $\alpha = 0.5$ under different liquid viscosity.

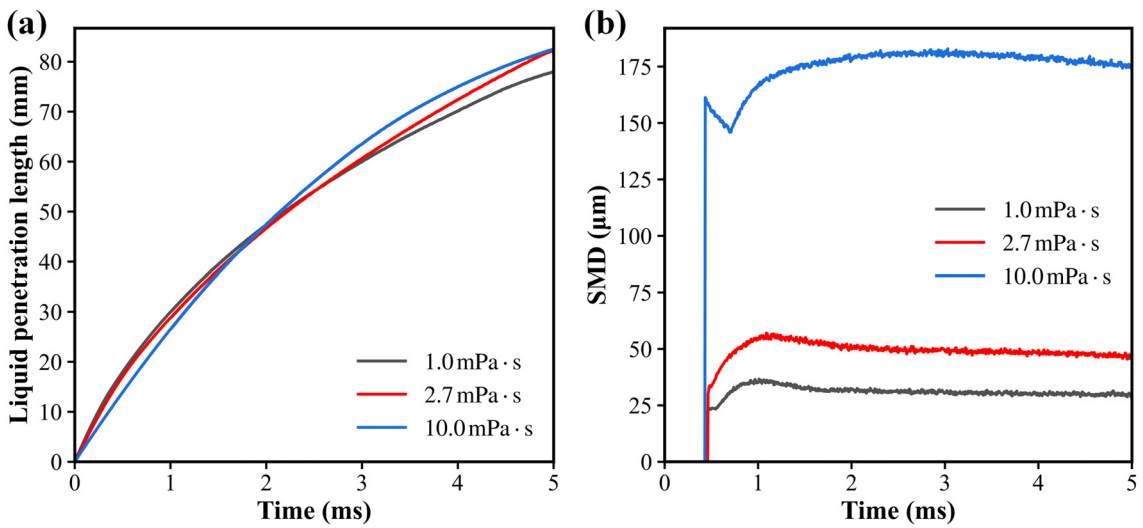

FIG. 17. Time evolution of (a) the liquid penetration length and (b) SMD under different liquid viscosity.

characteristics. As the convergence angle increases and the orifice length decreases, the length of the air core gradually decreases but the penetration remains slightly greater than the orifice length. There are asymmetric vortex structures within the air core inside the nozzle as indicated by the streamlines in Figs. 18(a) and 18(b). The position of these vortex shifts downstream when the air core tends to collapse on itself. When the orifice length decreases to 0.3 mm, the vortex within the air core disappears.

In addition, the effect of the diameter of swirl chamber and orifice (cases 10–12) is shown in Figs. 18(d)–18(f). The spray cone angle increases with the enlargement of the diameter of swirl chamber and orifice. At an orifice diameter of 0.4 mm, the air core collapses on itself resembling the low mass flow rate condition in Fig. 12(a). However, the aerodynamic interactions under high ambient pressures are stronger, leading to a more pronounced collapse of the liquid jet. Despite the fact that the spray cone angle is zero near the nozzle exit, the swirling liquid expanded the spatial distribution of the droplets. With an increase in diameter of swirl chamber and orifice, an air core gradually emerges and penetrates within the nozzle.

Figure 19 compared the liquid penetration and average SMD at 15 mm downstream of the nozzle exit under different nozzle geometry. Normally, the diameter of a fully developed air core increases with the shortening of the orifice length.[44] However, the air core failed to penetrate the entire nozzle under different nozzle geometries in this study, and the convergent angle also decreases simultaneously with the decrease in orifice length, leading to a shrinking air core region. When the orifice length decreased from 0.9 to 0.3 mm, the air core gradually collapsed, resulting in an increase in the calculated *Ca* from 0.0418 to 0.0488 based on Eq. (5). Therefore, the initial diameter of parcels which is equal to liquid film thickness increased from 122.67 to 132.54 μm. The high ambient gas density intensifies the interaction between the gas–liquid phases, resulting in minimal discrepancies in near-field SMD despite the different liquid film thicknesses for various orifice lengths.

The effect of the diameter of swirl chamber and orifice on external spray characteristics (cases 10–12) is shown in Figs. 19(c) and 19(d). The slope of the liquid axial penetration length reflects the axial velocity of the liquid film as shown in Fig. 18. With an increase in

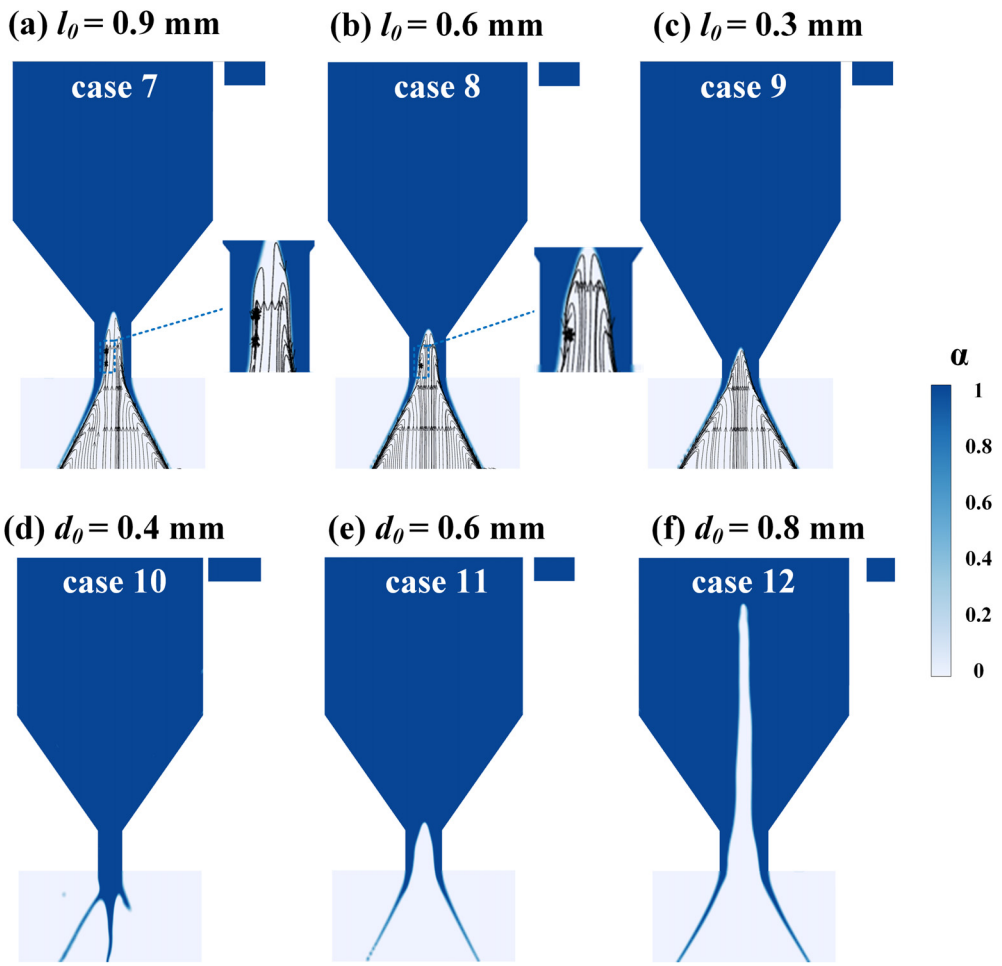

FIG. 18. Spatial distribution of void fraction under different nozzle geometry.

orifice diameter, the droplet velocity decreases. The near-field SMD decreases with the reduction of nozzle diameter. Interestingly, the nozzle with an absence of air core ($do = 0.4$ mm) achieves better atomization performance, yielding an approximate SMD of 22 μm at a quasi-steady state. This phenomenon is attributed to the significantly higher axial velocity of the liquid jet near the orifice compared to the hollow cone liquid film formed under other nozzle geometries, which operates at identical mass flow rate. Consequently, this intensifies the interaction between the spray and the high-density ambient air, resulting in more vigorous breakup and smaller droplet diameters.

V. CONCLUSION

In this study, a high-fidelity simulation of in-nozzle flow was performed for a pressure swirl atomizer, employing the VOF method coupled with the Geo-reconstruct algorithm to capture the sharp liquid–gas interface on a 13.64-μm-resolution computational mesh. Then, a novel Euler–Lagrangian one-way coupling method for hollow cone spray was proposed, wherein the injected parcels are initialized using the data from high-fidelity nozzle flow simulation. Both the internal flow and the spray characteristics results were validated with the experimental data available in the literature in terms of velocity distribution, liquid film thickness, spray cone angle, and SMD distribution. For different operation conditions and geometric parameters, the in-nozzle air core formation and hollow-cone spray characteristics were examined qualitatively and quantitatively. This result reveals the importance of in-nozzle flow that is usually ignored in spray simulations and provides more guidance for the PS atomizers design and spray model development. The conclusions are as follows:

(1) Compared with the conventional Lagrangian spray model, the developed one-way coupled model exhibits an error of 2.78% in predicting the spray cone angle, showing comparable predictive capability. However, the SMD predicted by conventional Lagrangian spray model is approximately 2.5 times the experimental values. Conversely, the developed one-way coupling model demonstrates very well predictions especially for the spray dense region, indicating a considerable enhancement in prediction accuracy.

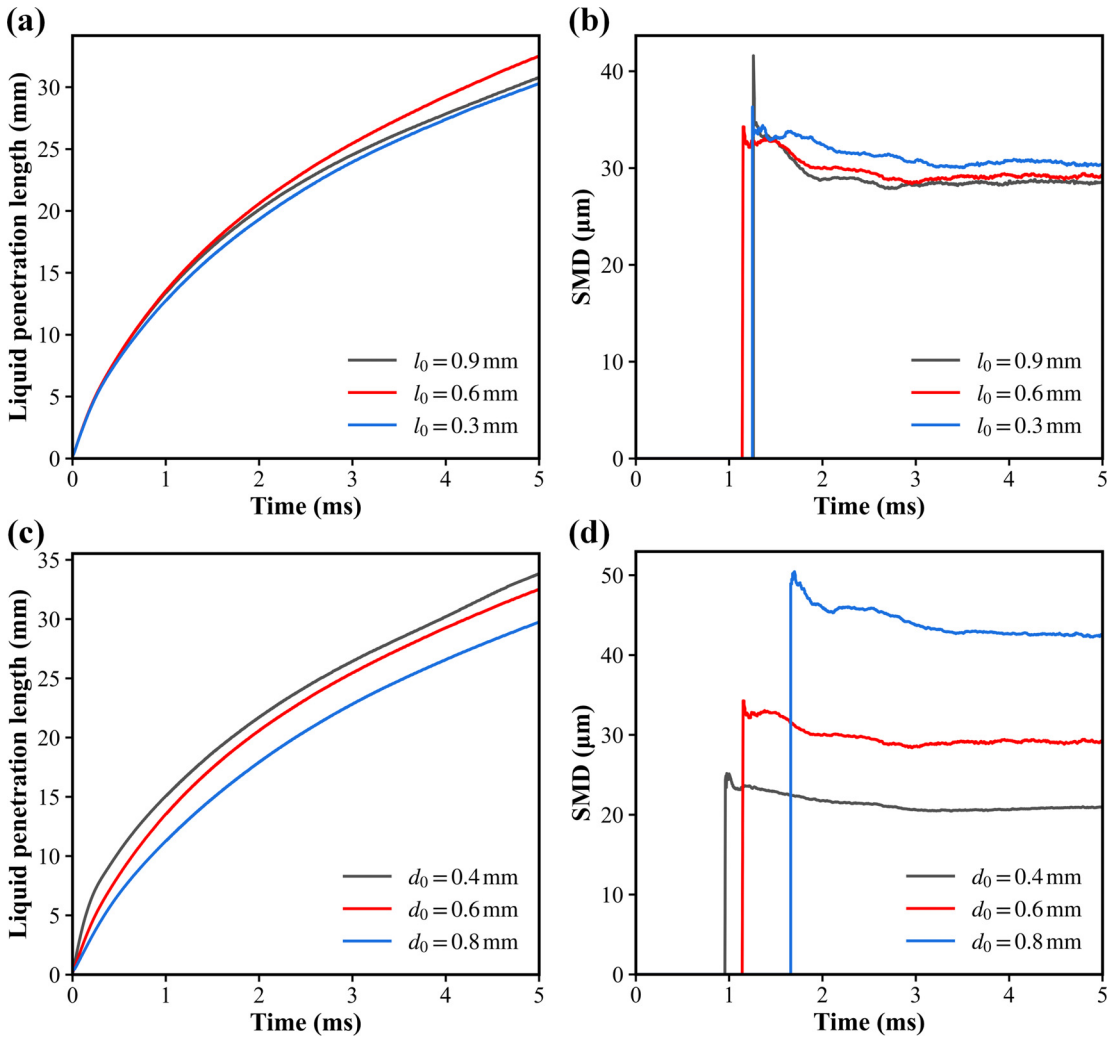

FIG. 19. Time evolution of (a) the liquid penetration length and (b) SMD under different nozzle geometry.

(2) The hollow cone liquid film from a pressure-swirl atomizer can degenerate into a solid cylindrical liquid jet under specific operating conditions and the degree of collapse increases with the increase in ambient pressure. With an increase in liquid mass flow rate, centrifugal forces gradually overcome viscous forces, causing ambient air to be drawn into the nozzle without rotational motion. Increasing liquid viscosity suppresses not only the formation of an air core but also the disturbances at the liquid–gas interface.

(3) When the air core fails to penetrate the entire nozzle under different nozzle geometry, the liquid film thickness gradually increases. Among these parameter variations (while keeping liquid mass flow rate constant), viscosity plays a vital role in the formation of the air core compared to pressure difference. As opposed to the converge angle and orifice length, the orifice diameter has a direct correlation with the formation of the air core and spray atomization.

ACKNOWLEDGMENTS

This work is supported by the National Natural Science Foundation of China (Grant Nos. 52006154 and 51921004) and Helan Turbines Co., Ltd.

AUTHOR DECLARATIONS

Conflict of Interest

The authors have no conflicts to disclose.

Author Contributions

Zongyu Yue: Conceptualization (equal); Formal analysis (equal); Funding acquisition (equal); Investigation (equal); Methodology (equal); Project administration (equal); Resources (equal); Supervision (equal); Writing – review & editing (equal). **Heng Liu:** Formal analysis (equal); Investigation (equal); Methodology (equal); Validation (equal);

Visualization (equal); Writing – original draft (equal); Writing – review & editing (equal). **Chuang Gao:** Funding acquisition (equal); Software (equal); Writing – review & editing (equal). **Song Cheng:** Software (equal); Supervision (equal); Writing – review & editing (equal). **Hu Wang:** Conceptualization (equal); Data curation (equal); Funding acquisition (equal); Project administration (equal). **Zunqing Zheng:** Funding acquisition (equal); Project administration (equal); Writing – review & editing (equal). **Mingfa Yao:** Funding acquisition (equal); Resources (equal); Supervision (equal); Writing – review & editing (equal).

DATA AVAILABILITY

The data that support the findings of this study are available from the corresponding author upon reasonable request.

REFERENCES

[1]J. Wang, Z. Wang, X. Hui, M. Han, C. Liu, and W. Tao, "The effects of fuel distribution on exit temperature distribution in a centrally staged combustor," Phys. Fluids **35**, 065136 (2023).

[2]T. Li, K. Nishida, and H. Hiroyasu, "Droplet size distribution and evaporation characteristics of fuel spray by a swirl type atomizer," Fuel **90**, 2367–2376 (2011).

[3]K. Nanan, K. Wongcharee, C. Nuntadusit, and S. Eiamsa-Ard, "Forced convective heat transfer by swirling impinging jets issuing from nozzles equipped with twisted tapes," Int. Commun. Heat Mass Transfer **39**, 844–852 (2012).

[4]W. He, Y. Zhao, and W. Fan, "Spray, flowfield, and combustion characteristics of an external mixing atomizer in a novel cavity-swirler-based combustor," Phys. Fluids **35**, 127115 (2023).

[5]K. Khani Aminjan, B. Kundu, and D. Ganji, "Study of pressure swirl atomizer with tangential input at design point and outside of design point," Phys. Fluids **32**, 127113 (2020).

[6]M. Halder, S. Dash, and S. Som, "Initiation of air core in a simplex nozzle and the effects of operating and geometrical parameters on its shape and size," Exp. Therm. Fluid Sci. **26**, 871–878 (2002).

[7]J. Cui, H. Lai, J. Li, and Y. Ma, "Visualization of internal flow and the effect of orifice geometry on the characteristics of spray and flow field in pressure-swirl atomizers," Appl. Therm. Eng. **127**, 812–822 (2017).

[8]X. Wei and H. Yong, "Improved semi-empirical correlation to predict sauter mean diameter for pressure-swirl atomizers," J. Propul. Power **30**, 1628–1635 (2014).

[9]R. Scardovelli and S. Zaleski, "Direct numerical simulation of free-surface and interfacial flow," Annu. Rev. Fluid Mech. **31**, 567–603 (1999).

[10]T. Wacławczyk and T. Koronowicz, "Modeling of the free surface flows with high resolution schemes," Chem. Process Eng. **27**, 783–802 (2006).

[11]Y. Liu, G. Liu, H. Xu, L. Chen, S. Qin, Y. Chao, and H. Zhang, "Research on breakup length and atomization characteristics of the swirl liquid sheet in perforation disintegration mode," Phys. Fluids **35**, 122123 (2023).

[12]J. K. Dukowicz, "A particle-fluid numerical model for liquid sprays," J. Comput. Phys. **35**, 229–253 (1980).

[13]Z. Yue and S. Som, "Fuel property effects on knock propensity and thermal efficiency in a direct-injection spark-ignition engine," Appl. Energy **281**, 114221 (2021).

[14]J. Sim, J. Badra, A. E. Elwardani, and H. G. Im, "Spray modeling for outwardly-opening hollow-cone injector," SAE Paper No. 2016-01-0844, 2016.

[15]A. Vallet, A. Burluka, and R. Borghi, "Development of a Eulerian model for the 'atomization' of a liquid jet," Atomization Sprays **11**, 24–642 (2001).

[16]F.-X. Demoulin, P.-A. Beau, G. Blokkeel, A. Mura, and R. Borghi, "A new model for turbulent flows with large density fluctuations: Application to liquid atomization," Atomization Sprays **17**, 315 (2007).

[17]S. Hoyas, A. Gil, X. Margot, D. Khuong-Anh, and F. Ravet, "Evaluation of the Eulerian-Lagrangian spray atomization (ELSA) model in spray simulations: 2D cases," Math. Comput. Modell. **57**, 1686–1693 (2013).

[18]K. Richards, P. Senecal, and E. Pomraning, *Converge (V3. 0)* (Convergent Science, Inc., Madison, WI, 2021).

[19]X. Liu, M. Al-lehaibi, and H. G. Im, "Investigation of the engine combustion network spray a characteristics using Eulerian and Lagrangian models," SAE Paper No. 2022-01-0507, 2022.

[20]K. Saha, S. Quan, M. Battistoni, S. Som, P. Senecal, and E. Pomraning, "Coupled Eulerian internal nozzle flow and Lagrangian spray simulations for GDI systems," SAE Paper No. 2017-01-0834, 2017.

[21]F. Wang, Z. He, J. Liu, and Q. Wang, "Diesel nozzle geometries on spray characteristics with a spray model coupled with nozzle cavitating flow," Int. J. Automot. Technol. **16**, 539–549 (2015).

[22]M. Al-lehaibi, X. Liu, and H. G. Im, "Numerical investigation of *n*-dodecane ECN spray and combustion characteristics using the one-way coupled Eulerian-Lagrangian approach," Fuel **331**, 125759 (2023).

[23]L. Nocivelli, B. A. Sforzo, A. Tekawade, J. Yan, C. F. Powell, W. Chang, C.-F. Lee, and S. Som, "Analysis of the spray numerical injection modeling for gasoline applications," SAE Paper No. 2020-01-0330, 2020.

[24]D. Ju, J. Deng, Q. Liu, J. Xia, S. Cheng, and W. Cai, "Experimental and computational analysis of n-decane spray characteristics discharged from a pressure-swirl nozzle into aeroengine-like conditions," Atomization Sprays **32**, 35 (2022).

[25]C. W. Hirt and B. D. Nichols, "Volume of fluid (VOF) method for the dynamics of free boundaries," J. Comput. Phys. **39**, 201–225 (1981).

[26]J. Chinn, "The internal flow and exit conditions of pressure swirl atomizers," Atomization Sprays **10**, 26 (2000).

[27]S. Kim, R. Torelli, S. K. Oruganti, J. I. Ryu, T. Lee, K. S. Kim, and C.-B. M. Kweon, "Modeling of the spray-induced wall stress acting on the ignition assistance device," Phys. Fluids **35**, 103325 (2023).

[28]X. Liu, P. Li, F. Li, C. Wang, X. Yang, H. Wang, M. Sun, Y. Yang, D. Xiong, and Y. Wang, "Effect of kerosene injection states on mixing and combustion characteristics in supersonic combustor at high equivalent ratio," Phys. Fluids **36**, 013305 (2024).

[29]F. Li, T. Wang, K. Yang, J. Zhang, H. Wang, M. Sun, Z. Wang, and P. Li, "Effect of fuel temperature on mixing characteristics of a kerosene jet injected into a cavity-based supersonic combustor," Phys. Fluids **35**, 043307 (2023).

[30]B. Bhatia, A. De, D. Roekaerts, and A. R. Masri, "Numerical analysis of dilute methanol spray flames in vitiated coflow using extended flamelet generated manifold model," Phys. Fluids **34**, 075111 (2022).

[31]J. Gao, M. F. Trujillo, and S. Deshpande, "Numerical simulation of hollow-cone sprays interacting with uniform crossflow for gasoline direct injection engines," SAE Int. J. Engines **4**, 2207–2221 (2011).

[32]J. C. Beale and R. D. Reitz, "Modeling spray atomization with the Kelvin-Helmholtz/Rayleigh-Taylor hybrid model," Atomization Sprays **9**, 623 (1999).

[33]A. A. Amsden, T. D. Butler, and P. J. O'Rourke, "The KIVA-II computer program for transient multidimensional chemically reactive flows with sprays," SAE Paper No. 872072, 1987.

[34]D. P. Schmidt and C. J. Rutland, "A new droplet collision algorithm," J. Comput. Phys. **164**, 62–80 (2000).

[35]M. Maly, J. Slama, O. Cejpek, and J. Jedelskỳ, "Comparison of numerical models for prediction of pressure-swirl atomizer internal flow," in International Conference on Liquid Atomization and Spray Systems (ICLASS), 2021.

[36]J. Jedelsky, M. Maly, N. P. Del Corral, G. Wigley, L. Janackova, and M. Jicha, "Air–liquid interactions in a pressure-swirl spray," Int. J. Heat Mass Transfer **121**, 788–804 (2018).

[37]K. Ghate and T. Sundararajan, "Effects of orifice divergence on hollow cone spray at low injection pressures," J. Aerosp. Eng. **233**, 4091–4105 (2019).

[38]C. Galbiati, S. Tonini, P. Conti, and G. Cossali, "Numerical simulations of internal flow in an aircraft engine pressure swirl atomizer," J. Propul. Power **32**, 1433–1441 (2016).

[39]P. Senecal, E. Pomraning, K. Richards, and S. Som, "Grid-convergent spray models for internal combustion engine computational fluid dynamics simulations," J. Energy Resour. Technol. **136**, 012204 (2014).

[40]Y. Chen, J. Luo, F. Wu, Z. Zhang, Z. Zhao, L. Zhang, C. Luo, and X. Li, "Multi-objective optimization on flow characteristics of pressure swirl nozzle: A LES-VOF simulation," Int. Commun. Heat Mass Transfer **133**, 105926 (2022).

[41]M. Maly, J. Jedelsky, J. Slama, L. Janackova, M. Sapík, G. Wigley, and M. Jicha, "Internal flow and air core dynamics in simplex and spill-return pressure-swirl atomizers," Int. J. Heat Mass Transfer **123**, 805–814 (2018).
[42]M. Di Martino, D. Ahirwal, and P. L. Maffettone, "Three-dimensional computational fluid dynamics simulation of the hollow-cone spray process: The stability of the conical liquid sheet," Phys. Fluids **33**, 063301 (2021).
[43]E. J. Lee, S. Y. Oh, H. Y. Kim, S. C. James, and S. S. Yoon, "Measuring air core characteristics of a pressure-swirl atomizer via a transparent acrylic nozzle at various Reynolds numbers," Exp. Therm. Fluid Sci. **34**, 1475–1483 (2010).
[44]Z. Kang, Z-g Wang, Q. Li, and P. Cheng, "Review on pressure swirl injector in liquid rocket engine," Acta Astronaut. **145**, 174–198 (2018).